npj | systems biology and applications

Article

Published in partnership with the Systems Biology Institute

https://doi.org/10.1038/s41540-025-00547-5

Personalized cancer treatment strategies incorporating irreversible and reversible drug resistance mechanisms

Wei He[1] ✉, Matthew D. McCoy[1,2], Rebecca B. Riggins[1], Robert A. Beckman[1,2,3] ✉ & Chen-Hsiang Yeang[4] ✉

Despite advances in targeted cancer therapy, the promise of precision medicine has been limited by resistance to these treatments. In this study, we propose a mathematical modelling framework incorporating cellular heterogeneity, genetic evolutionary dynamics, and non-genetic plasticity, accounting for both irreversible and reversible drug resistance. Previously we proposed Dynamic Precision Medicine (DPM), a personalized treatment strategy that designed individualized treatment sequences by simulations of irreversible genetic evolutionary dynamics in a heterogeneous tumor. Here we apply DPM to the joint model of reversible and irreversible drug resistance mechanisms, analyze the simulation results and compare the efficacy of various treatment strategies. The results indicate that this enhanced version of DPM significantly outperforms current personalized medicine treatment approaches. Our results provide insights into cancer treatment strategies for heterogeneous tumors with genetic evolutionary dynamics and non-genetic cellular plasticity, potentially leading to improvements in survival time for cancer patients.

Drug resistance remains a primary obstacle in cancer treatment[1]. Intratumoral genetic heterogeneity and non-genetic plasticity in cancer cells are two major factors of cancer treatment resistance[2–9], and are widely associated with poor outcomes and reduced responses to therapies[1,2,10–13]. A bulk tumor typically consists of a heterogeneous population of cancer cells often characterized by bulk or subclonal genetic instability[2,10,14–17]. By sequencing tumors with a higher depth and accuracy and applying a novel mathematical model, we found that every DNA nucleotide is mutated in at least one cell in the smallest tumor visible on CT (Computed Tomography), unless that mutation is highly selected against[14]. This implies that at least one cancer cell is likely resistant to any single drug therapy and already present in any tumor at diagnosis[14]. Elevated genetic mutation rates and selection imposed by treatments drive the clonal evolution of tumors toward resistance. Of note, it is likely that a subset of cells has mutations in the cellular machinery that normally ensures genetic stability. We have termed these subclones "hypermutator subclones," and they may be selected as single and multidrug resistance evolves[17]. In addition, non-genetic plasticity in cancer cells provides a rapid reversible mechanism for drug-induced resistance[13]. Cancer cells can increase drug efflux, alter drug metabolism and activate bypassing signaling pathways to become resistant to the drugs. These two types of drug resistance mechanisms – intratumoral genetic subclonal heterogeneity and non-genetic cellular plasticity and heterogeneity – differ in their reversibility and in their clinical correlates. The former is irreversible as a resistant subclone will rarely revert mutations to lose its phenotype before expanding, and then reversions will occur in only a minority of cells[18]. It is likely to cause moderate term to late progression or relapse as it may involve outgrowth of rare subclones, and/or the accumulation of multiple resistance mutations. The latter is reversible as cells can alter their internal states to adapt to changes in the microenvironment (e.g., presence or absence of drugs), hence resistance can be reversed when the drug treatment is discontinued[13,19–21]. This reversible resistance may occur rapidly in a majority of cells, and clinically may correspond to primary resistance and/or short term relapses.

Previously, we have proposed mathematical models and treatment strategies to address the irreversible and reversible mechanisms of drug resistance in separate studies[22–24]. For the irreversible mechanism, we constructed a model to capture the population dynamics of tumor subclones as they acquire resistance to two or more non-cross resistant drugs through independent mutations, and proposed a treatment selection strategy, Dynamic Precision Medicine (DPM) to design the treatment sequence to balance the immediate goal of shrinking tumor size and the long term goal of preventing the emergence of an incurable subclone resistant to both drugs[22].

[1]Department of Oncology, Lombardi Comprehensive Cancer Center, Georgetown University Medical Center, Washington, DC, USA. [2]Innovation Center for Biomedical Informatics, Georgetown University Medical Center, Washington, DC, USA. [3]Department of Biostatistics, Bioinformatics, and Biomathematics, Georgetown University Medical Center, Washington, DC, USA. [4]Institute of Statistical Science, Academia Sinica, Taipei, Taiwan.
✉e-mail: wh490@georgetown.edu; eniac1915@gmail.com; chyeang@stat.sinica.edu.tw

(Notably, many drugs are cross resistant. Such drugs are considered the same drug by DPM, and even when used in combination are treated as a single "drug"). DPM contrasts with the conventional precision medicine approach that attempts to match a drug (or a combination of drugs) to the molecular profile of a patient but does not address the complex relations between the patient's molecular profile, possible treatment sequences, and the dynamic response of the tumor. For the reversible mechanism, we introduced another mathematical model where cancer cells responded to the presence or absence of a drug by activating/inhibiting two alternative pathways, and proposed an optimal dynamic treatment strategy accordingly[24].

We now report a single, integrated mathematical model that captures both irreversible genetic drug resistance and reversible drug resistance induced by cellular plasticity. The unified framework encompasses both irreversible and reversible drug resistance for two non-cross resistant drugs, and the treatment strategies that simultaneously tackle the irreversible and reversible drug resistance mechanisms. We evaluate the effectiveness of nine treatment strategies by simulating the dynamics of cancer cell populations. We conduct a clinical trial simulation over 6 million virtual patients, each representing a different dynamic presentation at diagnosis, and demonstrate that the DPM-based personalized treatment strategies significantly outperform current personalized medicine treatment approaches. Furthermore, DPM strategies incorporating periodic treatment sequences that cycle between therapies over a shorter treatment window, designed to combat reversible resistance, are marginally superior to those without such options. There are a number of potential cases that may be captured by this generic modeling framework. As one example, the availability of several EGFR tyrosine kinase inhibitors (TKIs) for treatment of non-small-cell lung cancer (NSCLC) raises important questions about the optimal treatment sequence[25]. Afatinib, a TKI used for NSCLC, commonly encounters resistance through the T790M gatekeeper mutation, as well as mechanisms involving increased IL6R/JAK/STAT signaling enhanced autophagy[26]. On the other hand, osimertinib as another TKI, is highly selective for treating T790M-positive tumors following failure of prior EGFR TKI treatment and has shown remarkable efficacy in this setting[27]. Resistance mechanisms for osimertinib have also emerged, including *EGFR* mutations in L718V and G724S, HER2 amplification and RAS-MAPK pathway activation[28]. Interestingly, afatinib was successful in overcoming G724S-mediated resistance to osimertinib in vitro[29], and preclinical studies have shown that L718V mutation retains sensitivity to afatinib[30]. There are reports and clinical studies investigating the feasibility and exploring the optimal sequencing of these two EGFR TKIs[25,31–34]. Our model framework could potentially offer insights into a more effective treatment strategy for these two inhibitors by considering the reversible and irreversible resistance mechanism induced by these EGFR TKIs.

Mathematical models have been utilized to design effective treatment strategies aimed at addressing drug resistance[35–40]. Gatenby and colleagues proposed adaptive therapy, a strategy that dynamically adjusts treatment to preserve a population of drug-sensitive cells. These cells are proposed to compete with resistant ones, with the goal of controlling the tumor rather than fully eradicating it[41]. However, these sensitive cells continue to mutate and serve as a reservoir for future variants, and the competition between cells may be less of a factor in small metastatic sites that are usually the primary cause of death in patients[42]. Moreover, sensitive cells have in some cases been documented to support the fitness of resistant cells in co-culture[43,44]. Strobl et al. proposed that adaptive therapy could mitigate both the toxicity and resistance associated with poly-adenosine ribose polymerase inhibitor (PARPi)[37]. Gallagher et al. applied deep reinforcement learning to guide adaptive drug scheduling, demonstrating that such schedules could outperform the current adaptive protocols in a simulation of a mathematical model in a small cohort of virtual patients calibrated to prostate cancer, helping to delay the onset of drug resistance. Adaptive therapy has shown promising results in metastatic prostate cancer treating with a single drug[45]. However, sensitive and resistant cells were inferred in this model rather than measured, and it is possible that the therapy interruptions in adaptive therapy with a single agent are effective because they essentially promote a cycling approach, which can also be beneficial for managing reversible resistance, rather than due to competitive interactions between sensitive and resistant cells. Furthermore, deep learning algorithms are very powerful but are also limited by two critical factors for tumor therapeutics: the requirement for big training data and uninterpretable outcomes. Our approach aims to delay or prevent the appearance of doubly genetically resistant cell types and was one of the first to include sequencing of multiple non-cross resistant therapies by using multiple agents[22]. Zhou et al. explored non-genetic resistance mechanisms in colorectal cancer, demonstrating that resistant clones can regain sensitivity once therapeutic pressure is removed, highlighting phenotypic plasticity and reversibility[21]. Sahoo et al. explored the coupled dynamics of epithelial-mesenchymal transition (EMT) and the development of reversible drug resistance in breast cancer[46]. These models typically focus on a single resistance mechanism, either reversible or irreversible. In contrast, we propose a mathematical modelling framework incorporating both irreversible and reversible drug resistance. This approach enhances existing models by providing insights into treatment strategies for heterogeneous tumors, accounting for both Intratumoral genetic heterogeneity and non-genetic cellular plasticity.

Results

Our model incorporates two drugs where drug 1 corresponds to the first line treatment and is considered more effective than drug 2. There are potentially nine states in the model representing combinations of sensitivity (S), reversible resistance (T) and irreversible resistance (R) to the two drugs respectively as illustrated in Fig. 1 and Table 1. We consider nine treatment strategies which are shown in Fig. 2 such as S0 (strategy 0) representing current personalized medicine (CPM).

DPM and Cycle are the superior strategies for the irreversible resistance only and reversible resistance only models respectively

We first performed a qualitative check by demonstrating that the simulation outcomes on the degenerate model with irreversible resistance alone were similar to our previous study of DPM[22]. The results are consistent with our previous observation that DPM strategies S1 and S2 outperform the CPM strategy. Figure 3a displays the Kaplan-Meier curves of the five of the nine treatment strategies on 578884 virtual patients in the irreversible resistance only model. S1 (magenta) and S2 (purple) curves are significantly superior to S0 (green). In Supplementary Table 2 and Supplementary Figure 1, S1 and S2 have higher median survival time, mean survival time, number of cases of survival over 5 years, and number of cases with numerically longer survival time compared to S0. Supplementary Table 3 shows that the pairwise hazard ratios of S1 and S2 are much lower compared to S0. S2 is slightly better than S1 in terms of the aforementioned metrics, with a median survival time increase of 86 days, a mean survival time increase of 33 days, and an additional 14140 cases surviving over 5 years, resulting in a hazard ratio of 0.935 compared to S1. These outcomes mirror the results in the original simulation of the irreversible model[22], in which S2 was the superior strategy but had only a slight advantage over S1. Furthermore, by comparing the results between S1 and S1c and between S2 and S2c in Supplementary Table 2 and 3, we found that adding the cyclic treatment options to DPM strategies only marginally increased survival times (1-2% increase from S1 to S1c and 0.3% increase from S2 to S2c), and yielded pairwise hazard ratios near 1. The limited improvement by incorporating cycling treatment options into DPM is expected because cycling drug dosages are expected to be more effective on reversible resistance cell states, which are absent in the degenerate irreversible resistance only model.

Figure 4a-d illustrates the benefit of the DPM strategy (S2) in a virtual patient possessing a dominant sensitive (S_1S_2, ~90%) cell population and two minor, singly resistant (R_1S_2, ~10% and S_1R_2, <0.001%) cell populations initially. S0 (Fig. 4a) targets the dominant subclone (S_1S_2), thus chooses the more effective drug 1 in the first period. Sensitive (S_1S_2) and drug 2 resistant

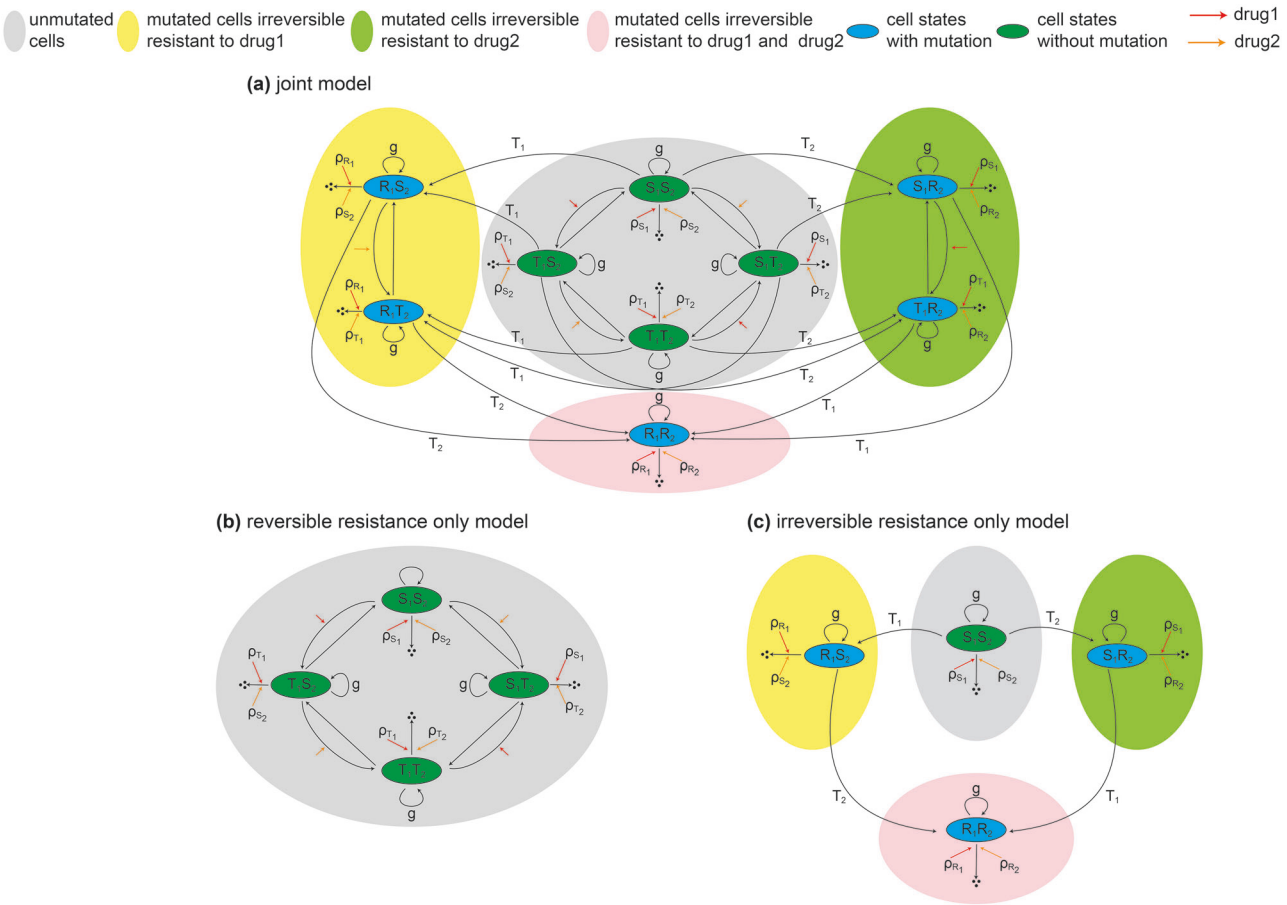

Fig. 1 | Overview of proliferations and transitions among different cell states and schematic representation of the structures of the mathematical model. a The joint model structure used for simulation, which illustrates the dynamics of multiple cell states and their transitions in the presence of drug 1 and drug 2. Cell states are represented by two symbols, corresponding to drugs 1 and 2, respectively; each of which is in one of the three possible states for each drug: sensitive to the drug (S), reversibly resistant to the drug (T), or irreversibly resistant to the drug (R). The central gray bubble comprises the state transitions of the reversible resistance only model where the irreversible resistance mutations do not occur. The left yellow bubble and the right green bubble comprise the state transitions where the irreversible resistance mutation of drug 1 or drug 2 alone occurs. The bottom pink bubble comprises the states possessing double irreversible resistance of both drugs. Arrows include self-replications, degradations and transitions/mutations from or to designated states. Model parameters are described in the text below. **b** the reversible resistance only model. **c** the irreversible resistance only model.

Table 1 | Cell state descriptions

Index	Cell state	Description
1	S_1S_2	sensitive to drug 1 and drug 2
2	T_1S_2	reversible resistant to drug 1 and sensitive to drug 2
3	S_1T_2	sensitive to drug 1 and reversible resistant to drug 2
4	T_1T_2	reversible resistant to both drug 1 and drug 2
5	S_1R_2	sensitive to drug 1 and irreversible resistant to drug 2
6	T_1R_2	reversible resistant to drug 1 and irreversible resistant to drug 2
7	R_1S_2	irreversible resistant to drug 1 and sensitive to drug 2
8	R_1T_2	irreversible resistant to drug 1 and reversible resistant to drug 2
9	R_1R_2	irreversible resistant to both drug 1 and drug 2

(S_1R_2) cells are drastically reduced, but drug 1 resistant (R_1S_2) cells rapidly proliferate and doubly resistant (R_1R_2) cells arise from the R_1S_2 cells by mutation in the first period. Hence the tumor becomes incurable and quickly reaches the mortal threshold. Zoomed-in views of the initial period of Fig. 4a is shown in Supplementary Figure 2a. S1 (Fig. 4b) attempts to minimize the predicted total population, thus chooses drug 2 in the first period because it reduces both sensitive (S_1S_2) and the abundant drug 1 resistant (R_1S_2) cells. The total population is minimized after the first period, but drug 2 resistant cells rapidly proliferate and doubly resistant cells also arise in the first treatment window. A combination of both drugs is administered in the second period to curb the two singly resistant cell populations, but the tumor is still incurable and quickly reaches the mortal threshold. S2 (Fig. 4c) attempts to prevent the emergence of doubly resistant cells, thus chooses two-drug combination in the first period to reduce both singly resistant cell populations. The doubly resistant cells do not arise, hence drug 2 is administered in the subsequent periods to eliminate drug 1 resistant cells. Zoomed-in views of the initial period of Fig. 4c is shown in Supplementary Figure 2b. Eventually the patient is cured. Figure 4d displays the trajectories of total cell numbers of the S0, S1, and S2 strategies. In previous work[22,23] we have found that initial simultaneous combinations are not always optimal, however; this depends on the detailed dynamics.

We performed the second qualitative check by demonstrating that the simulation outcomes on the degenerate model with reversible resistance alone were similar to our previous study of a reversible resistance model[24]. Figure 3b displays the Kaplan-Meier curves incorporating the four out of the seven treatment methods on 528 virtual patients in the reversible resistance only model. The Cycle and S1c treatment substantially outperform other strategies according to both Fig. 3b, survival time metrics in Supplementary Table 4, and pairwise hazard ratios in Supplementary Table 5. Moreover,

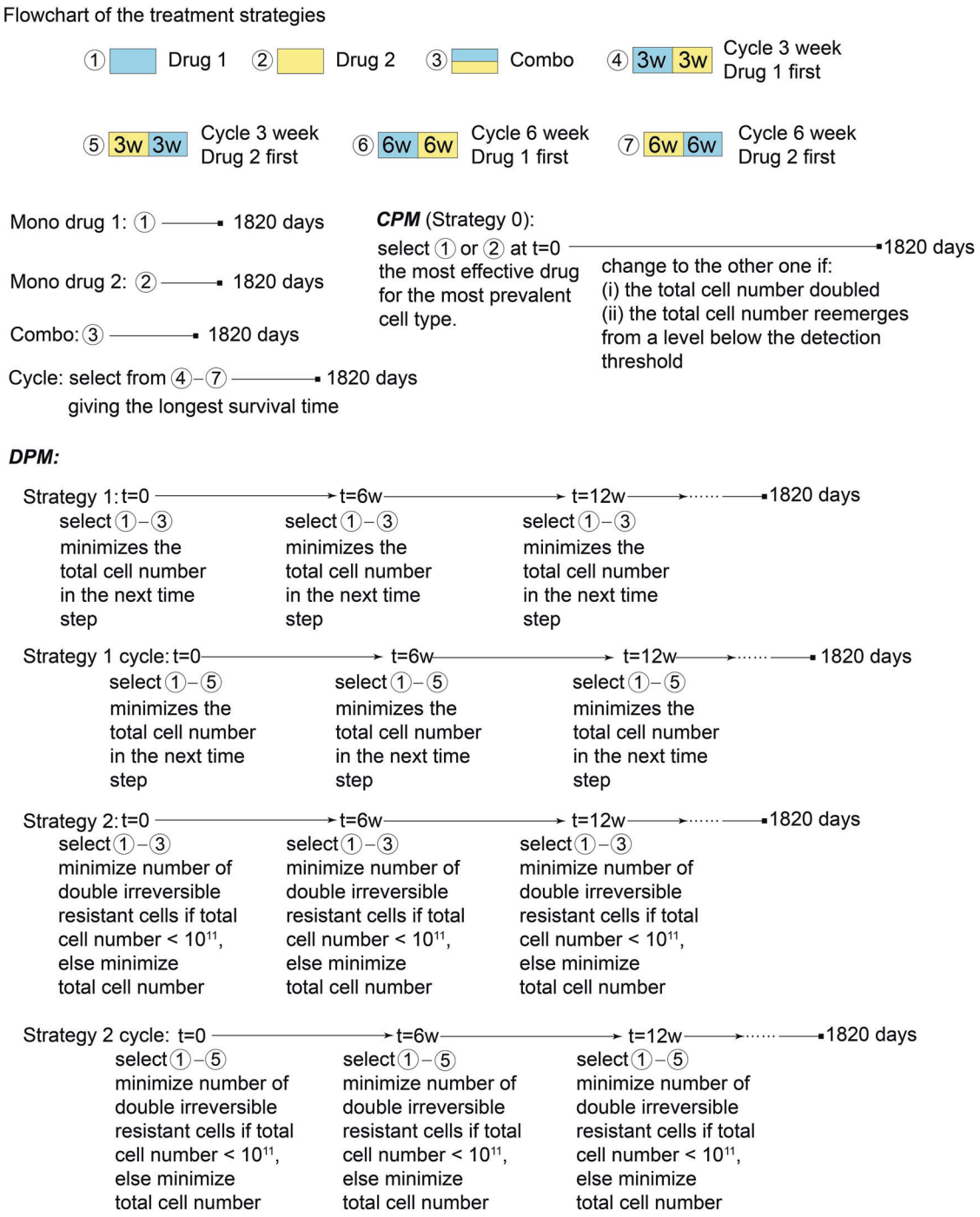

Fig. 2 | Flowchart of the treatment strategies. Flowchart of the nine treatment strategies outlined in the Methods section.

unlike the irreversible resistance only case, the mean survival time increases about 7% from 1394 days in S1 to 149 days in S1c, with a hazard ratio of S1c over S1 treatment of 0.725. These improvements corroborate the effectiveness of the cyclic treatments in tackling reversible resistance.

Figure 4e-g illustrates the effectiveness of the Cycle strategy in a virtual patient possessing a dominant sensitive (S_1S_2, ~99%) cell population, along with two minor singly reversible resistant (S_1T_2, ~0.02% and T_1S_2, ~0.02%) cell populations, and a smaller minor doubly reversible resistant (T_1T_2, ~0.00005%) cell population initially. S0 (Fig. 4e) drives transitions into the T_1T_2 cell state and yields a shorter survival time. By contrast, Cycle (Fig. 4f) pushes cells to oscillate between the two singly resistant states (S_1T_2 and T_1S_2) through the intermediate sensitive state (S_1S_2). This cycling ensures that there is always a period during which at least one of the drugs can kill the cells, and there is no overlapping period that allows the transition to T_1T_2 cells. Consequently, all cell populations gradually decrease, demonstrating that the Cycle treatment effectively controls the total cell number and outperforms other treatment methods. Figure 4g displays the trajectories of total cell numbers of the Cycle and S0 strategies.

Incorporating cyclic options into DPM-based strategies improve outcomes in the joint model

After confirming the effectiveness of DPM and cycling treatment in the degenerate models of irreversible and reversible resistance, respectively, we sought to demonstrate that the combination of these two approaches can tackle both irreversible and reversible resistance jointly. Figure 5a displays the Kaplan-Meier curves of four treatment strategies over 6131903 virtual

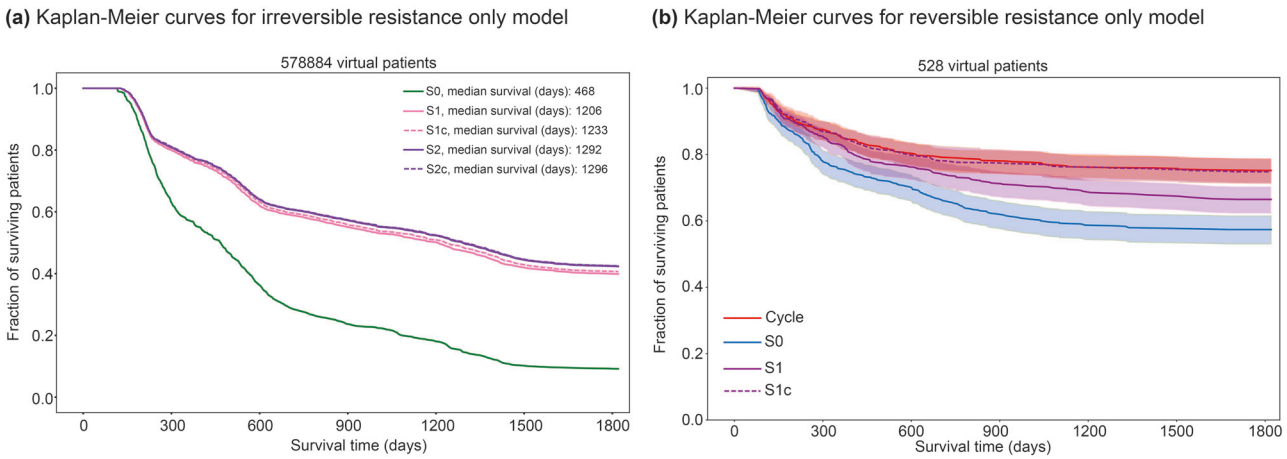

Fig. 3 | Kaplan-Meier curves of several treatment strategies in the irreversible and reversible resistance only model. a Kaplan-Meier curves of five treatment strategies over 578884 virtual patients in the irreversible resistance only model. **b** Kaplan-Meier curves of four strategies over 528 virtual patients in the reversible resistance only model. The shading surrounding each curve denotes a +/− 1 standard deviation range of simulations.

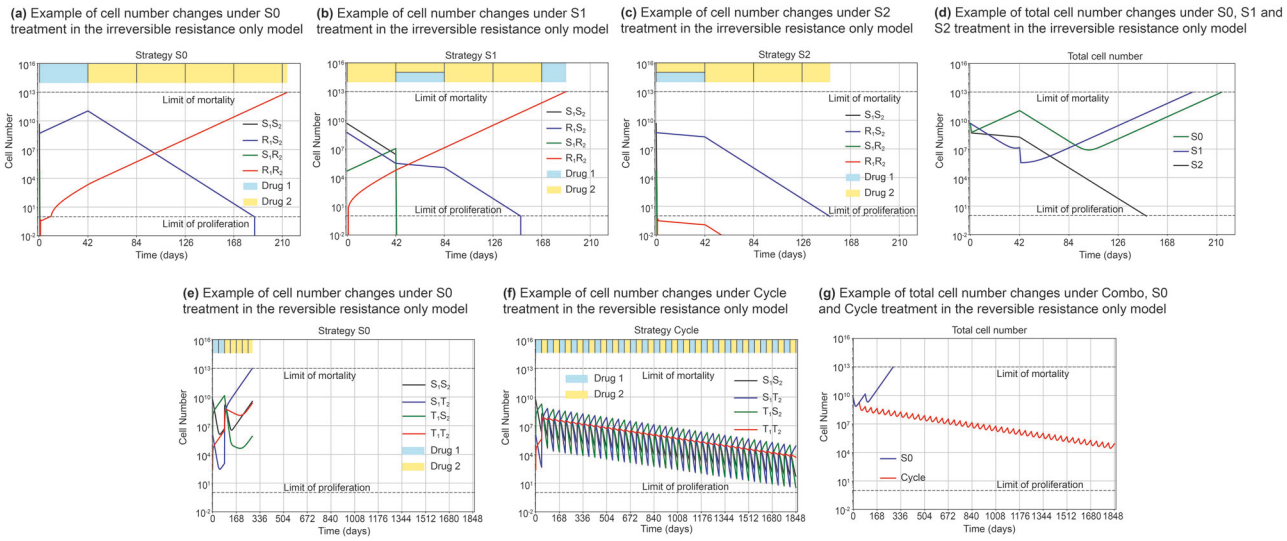

Fig. 4 | Population dynamics of illustrative virtual patients in the irreversible and reversible resistance only model. a–**d** Population dynamics of an illustrative virtual patient in the irreversible resistance only model contrasting S0, S1, and S2 treatment responses. Panels (**a**–**c**) display the population dynamics of individual cell types and dosage sequences under the three treatment strategies. The drug dosage in each treatment period is visualized by colored bars on the top row. Zoomed-in views of the initial periods of panels (**a** and **c**) are shown in Supplementary Fig. 2. Panel (**d**) displays the population dynamics of the sum of all cell types under the three strategies. **e**–**g** Population dynamics of an illustrative virtual patient in the reversible resistance only model contrasting S0 and Cycle treatment responses. Panel (**g**) displays the population dynamics of the sum of all cell types under the two strategies.

patients in the joint model (all nine strategies are displayed in Fig. S2). S1c (purple dashed) and S2c (red dashed) curves are superior to Cycle and substantially higher than S0 strategies. These two strategies also have higher median survival time, mean survival time and number of cases of survival over 5 years compared to the other strategies as shown in Table 2, and smaller pairwise hazard ratios as shown in Table 3. S2c is better on average than S1c based on the metrics in Table 2, with an additional 12312 cases surviving over 5 years. Relative performance of the two strategies varies in individual virtual patients based on the relative potency of the two drugs and other factors. In general, whether S1c or S2c are preferred may need to be individualized in subgroups of patients based on their drug sensitivities and evolutionary dynamics. The benefits of adding the cyclic treatment as a treatment option in each period are seen by comparing S1c/S2c with S1/S2 simulation outcomes in Table 2. S1c/S2c outperforms S1/S2 by 8% in terms of the median survival time, 9% and 7%, respectively, in terms of the mean survival time, and pairwise hazard ratios are ~0.92 for each. These improvements in the joint model but not in the irreversible resistance only model, though modest, underscore the effectiveness of cycling treatments in addressing reversible resistance mechanisms when both resistance mechanisms are present. Likewise, the benefits of introducing DPM to tackle irreversible resistance are seen, as the Cycle strategy (cycling drug 1 and 2 without DPM) has very similar outcomes to S1c and S2c in the reversible resistance only model (Supplementary Tables 4 and 5), but S1c and S2c are superior to Cycle in the joint model (Tables 2 and 3). Overall, comparing cycling, S1c and S2c, modest trends in average results are seen as described above. The benefits are more modest because the cancer model incorporates several distinct processes of resistance development, a greater challenge. Additionally, for 8479 patients, S0 performs significantly better than all other strategies (Table 2). But the strategy of choice depends on the dynamics in individual virtual patients in a complex way. It is expected that the benefits of a particular strategy will be seen more in subgroups of patients.

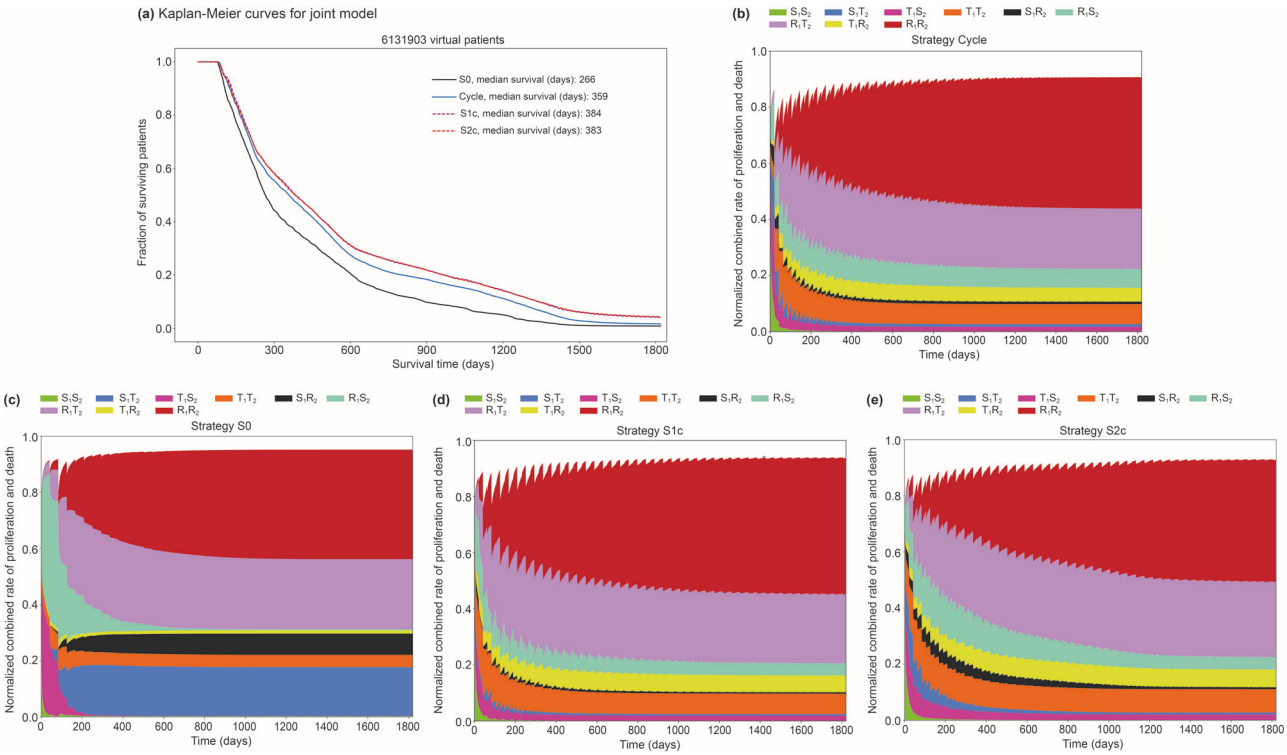

Fig. 5 | Kaplan-Meier survival curves and rates of each cell state change in the joint model incorporating different treatment strategies and normalized combined rate of proliferation and death for each cell state. 6131903 virtual patients were treated by each of the four treatment strategies. **a** Kaplan–Meier curves illustrating the simulated virtual patients. The y axis represents the fraction of surviving virtual patients. **b**–**e** Normalized net rates of proliferation and death for each cell state across all virtual patients under four treatment strategies Cycle (**b**), S0 (**c**), S1c (**d**) and S2c (**e**).

Table 2 | Comparison of treatment results in joint model

	Mono1	Mono2	Combo	Cycle	S0	S1	S1c	S2	S2c
Median survival	204	190	318	359	266	356	384	356	383
Mean survival	306	261	446	508	403	515	561	524	561
No. of cases survival over 5 years	0	0	0	105324	55737	167773	255938	188731	268250
No. of cases with numerically longer survival time than all others	0	0	1687	934105	17311	85174	1229424	149418	677783
No. of cases significantly better than all others	0	0	0	100	8479	76	3902	83	8440

Results are from simulation of 6131903 virtual patients in the joint model, with time measured in days.

Table 3 | The hazard ratio pairwise comparisons between different strategies in joint model

	Mono1	Mono2	Combo	Cycle	S0	S1	S1c	S2	S2c
Mono1	N.A.	0.82	1.623	1.88	1.417	1.891	2.083	1.919	2.076
Mono2	1.22	N.A.	1.928	2.212	1.699	2.228	2.437	2.259	2.429
Combo	0.616	0.519	N.A.	1.199	0.898	1.224	1.361	1.249	1.36
Cycle	0.532	0.452	0.834	N.A.	0.762	1.028	1.143	1.05	1.144
S0	0.706	0.589	1.114	1.313	N.A.	1.339	1.48	1.363	1.479
S1	0.529	0.449	0.817	0.973	0.747	N.A.	1.11	1.021	1.111
S1c	0.48	0.41	0.735	0.875	0.676	0.901	N.A.	0.92	1.001
S2	0.521	0.443	0.801	0.952	0.734	0.98	1.087	N.A.	1.088
S2c	0.482	0.412	0.735	0.874	0.676	0.9	0.999	0.919	N.A.

Results are from simulation of 6131903 virtual patients in the joint model. Row strategies are compared to the column strategies.

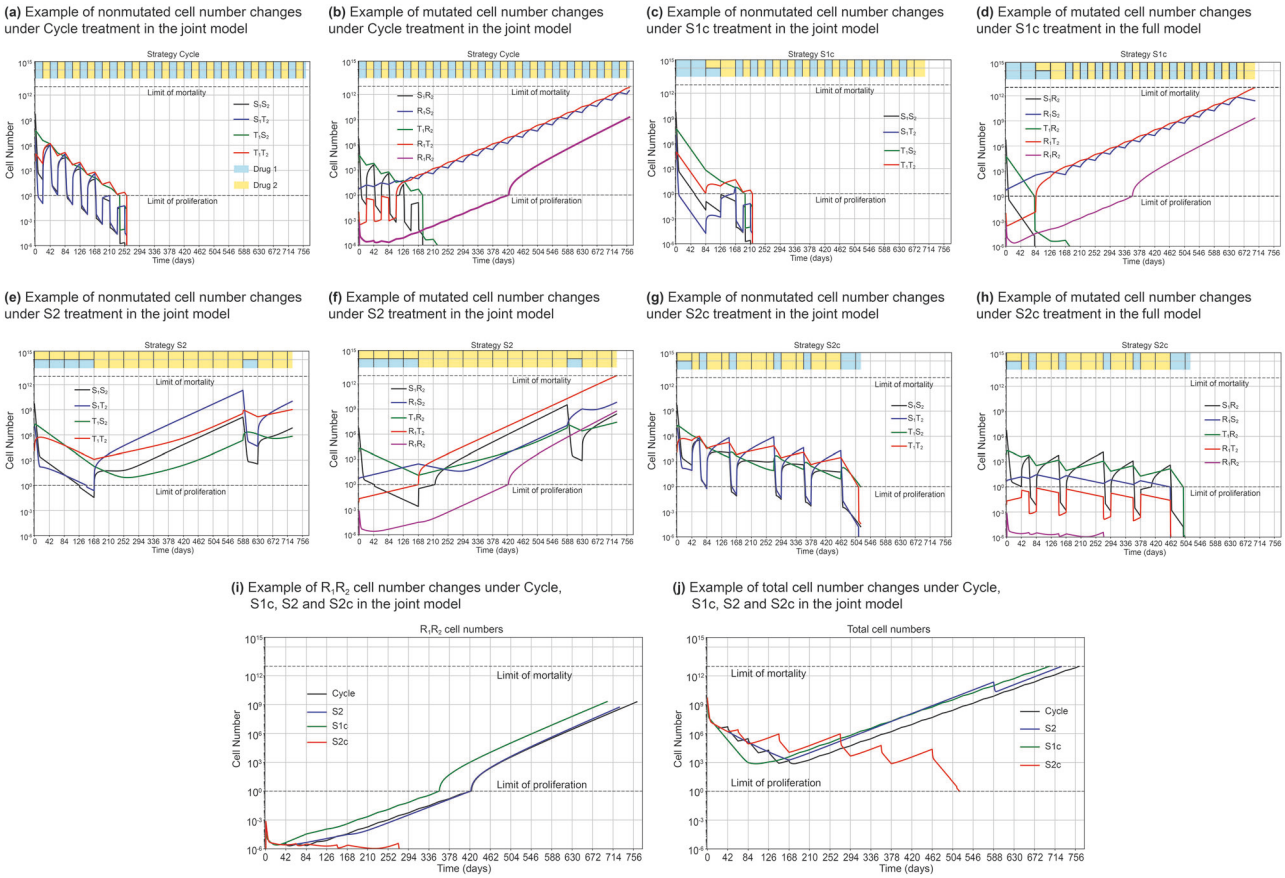

Fig. 6 | Population dynamics of an illustrative example contrasting four treatment strategies in the joint model. The visual representation in each panel is the same as Fig. 2c-j. The dynamics of nonmutated and mutated cell numbers are displayed for simulations under the Cycle strategy (**a** and **b**), S1c (**c** and **d**), S2 (**e** and **f**), and S2c (**g** and **h**). The dynamics of doubly mutated R_1R_2 and total cell numbers under the four strategies are displayed in (**i**) and (**j**) respectively.

Beyond survival outcomes, we are also interested in exploring the influence of treatment strategies on cell type composition dynamics. As a crude metric to capture the average composition dynamics, we calculate the net rate of cell number change for each cellular state (proliferation – death) at each time interval, normalized by the rates of all cell states and over all virtual patients. This metric quantifies the proportion of cells arising at each time interval rather than the accumulated cell numbers up to the specific time, and also takes an average over the trajectories among all virtual patients. Figure 5b–e displays the cell type composition dynamics of four treatment strategies: S0, Cycle, S1c, and S2c. All treatment strategies have rather smooth temporal profiles in their composition dynamics (except for the ripples for the strategies incorporating cycling treatments and the slightly more complicated profiles initially for S0). S0 (Fig. 5c) mainly selects drug 1 initially and then switches to drug 2 without switching back, hence the major cell types at steady state are resistant to drug 2, including S_1T_2, T_1T_2, S_1R_2, R_1T_2 and T_1T_2. For the other three strategies, the major cell types at steady state are R_1R_2 and R_1T_2. These strategies switch back and forth between drugs 1 and 2, leading to cells that are resistant to both drugs. The relatively small portion of T_1R_2 cells compared to R_1T_2 cells might be due to the higher potency of drug 1 compared to drug 2, where cells require mutations of drug 1 to survive. S2c also has a relatively lower portion of R_1R_2 cells compared to Cycle and S1c. This is because S2c is designed to specifically target and minimize the emergence of doubly irreversible resistant cells.

In Fig. 6, we present an example of a virtual patient where S2c yields the longest survival time. Figure 6a-b display the dynamics of non-mutated and mutated cell populations for the Cycle strategy. In Fig. 6a, Cycle effectively eliminates non-mutated cells such as S_1S_2, S_1T_2, T_1S_2 and T_1T_2. In Fig. 6b, Cycle cannot eliminate cells that are irreversibly resistant to drug 1 in this case. Although drug 2 has the potential to eradicate these cells, it fails to do so since it is only used with a 50% duty cycle. In Figs. 6c and 6d, the dynamics of cell states changes under S1c are similar to the changes under Cycle, where the emergence of R_1T_2 cells contribute to treatment failure. In S1c, after about four time steps, the strategy also selects cycling between drug 1 and drug 2 to minimize total cell numbers. The cell state changes under S2 and S2c are shown in Fig. 6e-h. The primary difference between S2 or S2c and Cycle or S1c is that S2 and S2c don't fully eliminate non-mutant cells. Instead, they aim to minimize the number of R_1R_2 cells, which indirectly minimizes the R_1T_2 cell numbers since this cell type, with irreversible resistance to drug 1 and reversible resistance to drug 2, is not readily treatable and will eventually mutate to R_1R_2 cells. In our model, a cell state can only proliferate when its cell number is >1. Therefore, S2 and S2c try to prevent the formation of the first R_1T_2 cell. S2 and S2c begin with a combination treatment where drug 2, the less potent drug, is included from the start. S2 treatment has fewer options and fails to prevent the formation of the first R_1T_2 cell. However, S2c can use cycling treatment to successfully avoid the formation of R_1T_2 cells, ultimately providing a cure. It is also notable that the first 2 or 3 time steps might be crucial for the ultimate treatment outcome, as shown for the irreversible DPM model as well[47]. Once the first incurable cell emerges, all drug treatment options become ineffective, leading to eventual mortality.

Numerically best treatment strategy changes when extending single resistance models to the joint model; and survival times vary depending on different parameter values

Each virtual patient parameter in the joint model can be generated by expanding one corresponding parameter from either of the degenerate models. A virtual patient from the irreversible resistance only model can be

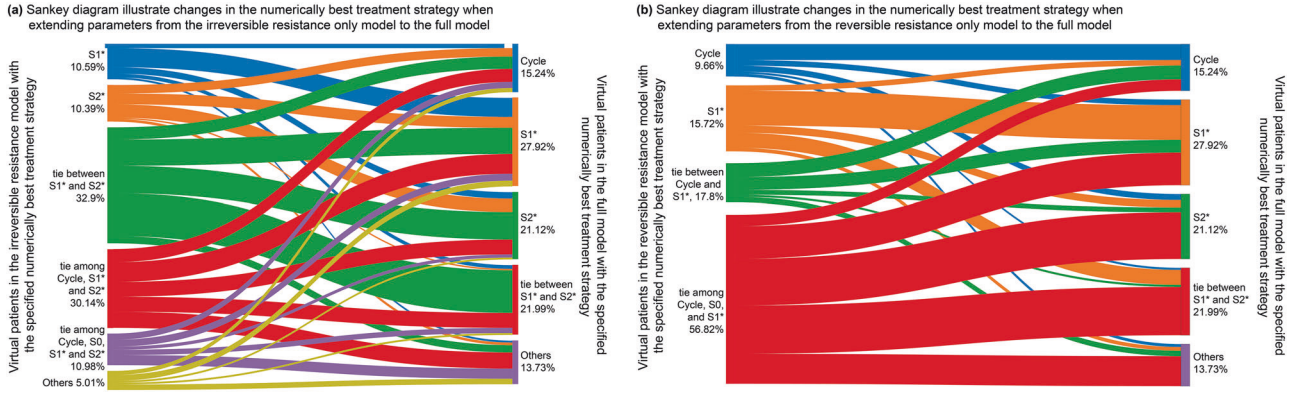

Fig. 7 | Sankey diagrams illustrate the changes of superior treatment strategy for the virtual patients when extending the degenerate model to the joint model. **a** Illustrates the changes in the numerically best strategy when extending each virtual patient from the irreversible resistance only model (left side) to the joint model (right side). **b** Illustrates the changes in the numerically best strategy when extending each virtual patient from the reversible resistance only model to the joint model. S1* represents either S1 or S1c treatment. S2* represents either S2 or S2c treatment. Others represents all the other possibilities except those listed in the degenerate model or joint model respectively.

extended into virtual patients in the joint model by incorporating parameters $\alpha_1, \theta_1, \mu_1, \alpha_2, \theta_2, \mu_2, ST_1$ and ST_2. Similarly, a virtual patient from the reversible resistance only model can be extended into virtual patients in the joint model by incorporating parameters $T_1, T_2, SR_1, SR_2, R1_{ratio}$ and $R2_{ratio}$. For a virtual patient in a degenerate model, there is a numerically best treatment strategy or strategies. In Fig. 7, we used Sankey diagrams to show that the numerically best treatment strategy changes when extending from a single resistance model to the joint model. S1* represents either S1 or S1c treatment, and S2* represents either S2 or S2c treatment.

When extending the virtual patients from the irreversible resistance only model to the joint model, the numerically best treatment strategies diverged, as shown in Fig. 7a. For instance, virtual patients who achieved the longest survival time under S2* treatment diverged to different treatment strategies (Supplementary Table 6). These changes are due to the incorporation of reversible resistance into the virtual patients and depend on the strength of the resistance. If the introduced reversible resistance is strong, the Cycle treatment is preferred as it can effectively tackle the reversible resistance. Similarly, when expanding the virtual patients in the reversible resistance only model to the joint model, the numerically best treatment strategies also diverged as shown in Fig. 7b (Supplementary Table 7). These changes are due to the incorporation of irreversible resistance into the virtual patients and depend on the strength of the resistance. The numerically best strategies for individual patients cannot be determined by a single resistance mechanism or predicted solely by the parameters related to one type of resistance in our virtual patient cohort. Instead, they are influenced by the interplay between the two resistance mechanisms, highlighting the necessity of building a unified framework that encompasses both irreversible and reversible drug resistance to identify treatment strategies that effectively address both mechanisms simultaneously.

Finally, we performed a sensitivity analysis of survival time outcomes in the joint model, demonstrating their dependence on varying parameter values. For each compared parameter or a parameter set (α, θ, μ), we fixed other parameters to the values corresponding to an original virtual patient and calculated the difference of survival times of pairs of virtual patients wherein the one parameter set was incremented or decremented as described in Methods. We consider α, θ, μ, as a single parameter set. If any of these three values differ between two virtual patients, we compared their survival times. For each parameter of T_1, T_2, ρ_{S_2}/ρ_{S_1}, SR_1 and SR_2, if the values between two virtual patients differ by one level as detailed in Supplementary Table 1, we compared their survival times. Figure 8a illustrates the changes in survival time when varying the parameters α, θ and μ, which determine the transition rate between the sensitive and reversible resistant states. These transitions are leveraged by cycling treatments to create opportunities to target and eliminate drug sensitive cells. Monotherapies appears to be less sensitive to these parameters, whereas strategies incorporating cycling treatments are more sensitive. Figure 8b shows the model's sensitivity to the ratio of ρ_{S_2} over ρ_{S_1} which specifies the efficacy of drug 2 compared to drug 1. Mono 1 is insensitive to drug 2, and all the other strategies have similar sensitivity to this ratio. Figure 8c illustrates the model's sensitivity to T_1 and T_2. Most the Mono treatments are less sensitive to these transition rates since either the initial resistant subclones will quickly dominate, or the reversible resistance will develop more rapidly. Figure 8d illustrates the model's sensitivity to SR_1 and SR_2, the relative sensitivity of the irreversible resistant phenotype to drugs 1 and 2 respectively. Mono 2 is unaffected by SR_1 and Mono 1 is unaffected by SR_2. Overall, the configuration of parameters for each individual virtual patient will influence the outcomes of the treatment strategies, resulting in varying survival times based on different parameter values.

Discussion

In this paper, we develop an integrated mathematical model, DPM-J that incorporates both irreversible and reversible resistance mechanisms for two non-cross resistant drugs or drug combinations. We evaluate the effectiveness of nine strategies for developing highly adaptive, individualized treatment sequences, by simulating the tumor growth and evolution of six million virtual patients each corresponding to a different set of input parameters. We confirm earlier findings that DPM-based strategies can improve clinical outcomes in a model including only irreversible genetic resistance. We also see an improvement when employing cycling of therapy for non-DPM-based strategies, presumably because this helps with diminishing reversible resistance. Our simulation results demonstrate that a combination of the DPM strategy and the cyclic dosages as a treatment option at each period can tackle irreversible and reversible resistance mechanisms simultaneously and hence yields the best performance. The joint treatment strategy takes advantage of the different time scales of reversible and irreversible resistance mechanisms. Knowledge of the reversible resistance kinetics generates optimal cycling building blocks in shorter treatment windows. These short term building blocks are then arranged in an optimal sequence by DPM to address moderate to long term issues.

The interplay between the internal states of cancer cells and the external conditions exerted by the drug dosages has the potential to produce a variety of population dynamics depending on the dosage sequence. Population dynamics are driven by both long-term irreversible and short-term reversible drug resistance mechanisms. In the long term, sensitive and resistant phenotypes manifest differential net growth rates in response to the administered drugs, and transition rates from sensitive to irreversible resistant phenotypes are treated as independent of the drug dosages. The

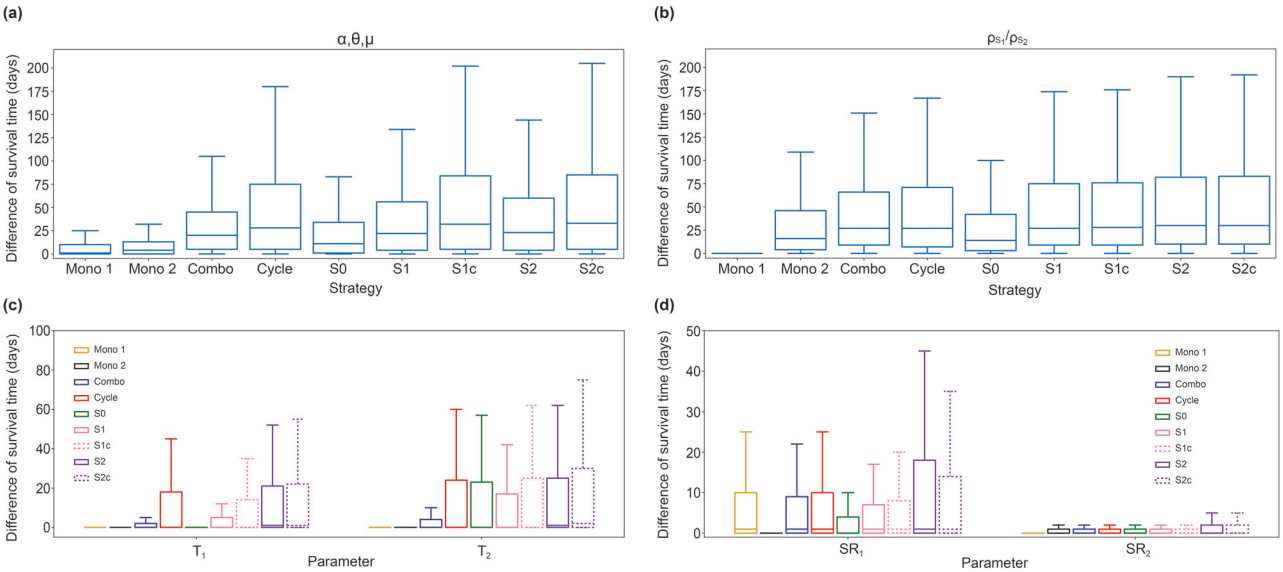

Fig. 8 | Boxplots illustrating the sensitivity analysis of survival time to the parameters in the joint model. Difference of survival time is on the y axis. **a** α, θ, μ, (α_1 equals α_2, θ_1 equals θ_2, μ_1 equals μ_2, respectively). **b** ρ_{S_2}/ρ_{S_1}. **c** T_1 and T_2. **d** SR_1 and SR_2.

genetic transitions of these abstract phenotypes can be attributed to all possible genetic mutations that induce the irreversible resistance phenotype. Drug dosages affect population dynamics by eliminating (or reducing) the sensitive subclones hence selecting the resistant subclones. In the short term, drug treatment inhibits the targeted pathway activity and kills the sensitive cells, but it also facilitates the activation of alternative pathways, leading to transitions that induce drug resistance (tolerance). When a drug treatment is withdrawn, the targeted pathway is no longer inhibited, hence the cells likely transition back to the sensitive state. The transition rates between these reversible states thereby depends on the drug dosage.

This work builds upon our previously proposed DPM treatment strategy[22]. DPM is a heuristic and parsimonious model. The model is primarily grounded in oncology principles but, like others, also draws on analogies to species evolution. However, species evolution and cancer evolution may be analogous but not identical, and DPM does not solely rely on these analogies. Species evolution typically occurs with a lower mutation rate[48], making the infinite sites approximation that a new mutation at a given base will appear only in one cell at any given time, widely applicable in that context. But this approximation may not hold in cancer where the mutation rate is higher[9,14]. Moreover, cancer evolution is not limited to a single ecological niche, but the niche is continuously expanding and diversifying through multiple metastases and micrometastases, a non-equilibrium situation[42]. Finally, competitive dynamics may differ in micrometastases below the angiogenic limit in size, which can be fully nourished by diffusion[42], reducing the importance of intercellular competition for nutrients. These micrometastases are often part of diffuse organ infiltration and associated with and/or causal of mortality. Moreover, in the high risk neoadjuvant setting, micrometastases may also be present below the level of radiologic detection. DPM considers these points and the total burden throughout the patient, rather than large lesions alone. DPM is also distinguished by its attention to rare subclones and hypermutator subclones. The former accounts for the possible different competitive dynamics, including independent growth in different ecological niches, by not assuming that rare subclones will be driven to extinction by competition. The latter considers that evolution rate will vary between subclones, a critical aspect of dynamics.

The myopic nature and limitations of CPM (S0 in our terminology) for cancer treatment have been criticized and addressed in abundant prior studies, including ours. S0 targets the dominant cell population at each moment, hence often discards the treatment sequences that are suboptimal in the short term but beneficial in the long term. Evolution guided precision medicine models[22–24,35–41], of which DPM is one example, consider intratumoral heterogeneity and dynamics in an attempt to improve upon current precision medicine in a proactive fashion. These approaches have not to date considered the coexistence of drug resistance mechanisms at different time scales in the same framework. Drug resistance phenotypes can be acquired by irreversible mutations or nearly irreversible epigenetic reprogramming, or achieved by reversible switching of the gene regulation/metabolic/signaling pathway activities. Previously, we modeled each type of drug resistance mechanism and provided effective or optimal treatment strategies to tackle them in separate works[22,24]. In this study, we explicitly model these two mechanisms together and provide a simple but effective heuristic to combine them. In the short term (within a treatment period of 6–12 weeks), physicians have options of administering the full dose of single drugs, reduced dose of both drugs (to model enhanced toxicity in simultaneous combination), or alternating the full dose of the two drugs in 3 week or 6 week cycles. In the long term (across multiple treatment periods), physicians employ the DPM algorithms (S1 or S2) to design the higher order treatment sequences. DPM may prevent or delay relapse or progression, while cycling may improve response rate and duration. To our knowledge, this is one of the first modeling approaches and treatment strategies for incorporating both irreversible and reversible resistance mechanisms in the same model for two-drug treatment of tumor population dynamics.

The benefits of cycling and of DPM on average remain quite significant compared to the standard precision medicine approach. Yet compared to each other cycling and DPM based strategies are more modestly differentiated from each other than seen in the simpler cancer models that considered only reversible resistance or only irreversible resistance. This is expected because the greater complexity of the model creates a greater challenge. Moreover, the optimal strategy is a complex function of the underlying drug properties, heterogeneity, and dynamics. This implies the need to carefully define patient subgroups for whom a given approach will be most optimal, and create evolutionary classifiers to sort individual patients into optimal evolutionary-guided strategies. We have made significant progress in this effort in predicting which patients in the irreversible resistance only model will benefit most from DPM[47].

DPM is designed to use approved drugs at approved dosages, either individually or in simultaneous combination, as deemed safe based on clinical studies. Drugs that are cross-resistant are treated as a single "drug" by DPM, even when used in combination. A "drug" in this context refers to either a single agent or a simultaneous combination of agents designed to target a specific class of subclones, with agents within the same drug

potentially being cross-resistant. Oncologists must nominate at least two non-cross resistant "drugs", and administering more than one non-cross resistant drug simultaneously often requires dose reduction due to toxicity. DPM is likely to be effective only in patients who do not already harbor cells with independent genetic resistance to both drugs. It is important to note that no current approach is likely to be effective if cells preexisting in the patient are already resistant to all available therapies. In the current DPM modeling framework, the mutation rate is assumed to be independent of drug treatment. However, we acknowledge that certain drugs, particularly some chemotherapeutic agents, can elevate mutation rates[49,50]. These mutagenic drugs have been shown to increase the number of mutations in cancer cells[51]. This effect could be incorporated into the model by modifying the mutation rate constant with a dose dependent factor to reflect the influence of drug exposure on mutation rates. In addition, our deterministic model using continuous variables may not fully capture the probabilistic dynamics of very small numbers when a subclone is close to elimination. While the model prevents the appearance of a subclone by keeping its number below one, in fact one or more cells could arise by stochastic fluctuations.

DPM and DPM-J are early in translational development in the laboratory. For DPM, we have recently described a number of translational advances including how one would select patients who will benefit in a clinical trial of the strategy, how long a period is required to obtain most of the benefit with maximal cost-effectiveness and minimal invasiveness, and some information on potential clinical trial designs[47]. DPM and DPM-J may recommend focusing on minor subclones for brief periods, while accepting a limited degree of what would be termed "progression" by standard radiologic criteria[52]. This approach should currently be undertaken only in the context of a clinical trial designed to evaluate the effectiveness of DPM based strategies. Moreover, in the simulation, the cancer burden threshold for reverting to prioritization of immediate cytoreduction is set a fixed value. However, in clinical practice, oncologists would determine when to prioritize additional cytoreduction based on the individual patient's context including the cancer type and many other factors.

Complex mathematical models present additional challenges for clinical translation[42]. Development approaches to individually parameterize the model with rapid turnaround time for clinical settings is ongoing. To parameterize the model, parameters can either be directly measured from patient data or inferred from it by fitting the data. Ideally, biopsies or highly sensitive and specific assays are needed to detect rare subclones individually and assess their drug sensitivity and resistance properties. Isolation of subclones is currently a barrier to this, especially rare subclones, and they often do not grow out at limiting dilution. Growth, sensitivity, and reversible transition rates can be either measured or estimated from growth data in the presence and absence of drug and under intermittent therapy. We have determined mutation rates from duplex sequencing data at varying sequencing depths[14]. This approach requires only a single timepoint and ~10 kb of DNA. We do not look for specific mutations, but rather the increase in the number of detectable mutations as a function of sequencing depth. We are also developing a fluorometric assay to identify a subpopulation of hypermutator cells in a bulk tumor sample. The assay would require transfection with the fluorophore construct, brief culture, and flow cytometry readout[53,54]. Mutation rates can also be estimated from fluctuation assays, and model parameters estimated from clinical data[55], with periodic reassessment if future states deviate from predictions.

Experimental and clinical validation of our treatment selection strategies will be essential in the future. Our current model should be viewed as a framework that accommodates generic drug resistance mechanisms rather than a realistic model for specific cancer types, targeted drugs, and involved pathways and genes. One promising test case for our model framework is triple positive breast cancer (TPBC). TPBC co-expresses two oncogenic drivers, estrogen receptor alpha (ER) and human epidermal growth factor receptor 2 (HER2). Multi-agent adjuvant anti-HER2 and -ER treatment is the superior approach for early stage and advanced or de novo metastatic TPBC[56–58]. However, outside academic medical centers a large subset (36.7-60%) of TPBC patients receive single agent anti-ER treatment[59,60]. Reanalysis of a large-scale study of advanced, endocrine-resistant breast cancer[61] shows that TPBC is overrepresented in those with the highest fraction of their genome altered ($q = 6.77e\text{-}9$). These genetic, irreversible resistance mechanisms are accompanied by well-known examples of reversible resistance[62–65]. We anticipate future implementation of this framework will lead to fruitful results in experimental validation and eventually improve treatment outcomes for this and other cancer types.

Methods

Model overview

We developed a joint mathematical model that incorporates both reversible and irreversible resistance mechanisms to simulate virtual patients' outcomes under different treatment strategies. We give a high-level overview of the model here and provide more precise descriptions in the subsequent sections. The irreversible and reversible portions of the model are primarily based on our prior studies[22–24]. The model includes two drugs, drug 1 and drug 2. In the irreversible part of the model, response of each drug in a cancer cell is indicated S (sensitive) or R (irreversible resistance), and drug resistance is acquired by the mutation of a gene (or one of a group of genes). There are four phenotypes in combination and we denote them by: S_1S_2, S_1R_2, R_1S_2, R_1R_2, representing the phenotypes sensitive to both drugs, resistant to drug 2, drug 1, and both drugs, respectively. These four cell types manifest differential death rates induced by drug dosages, and only mutations from sensitive to resistant phenotypes are allowed. In the reversible part of the model, the net growth rate (the proliferation rate minus the death rate) of a cancer cell can be activated by two distinct pathways. The two drugs target the two pathways by inhibiting their activities. There are also four cellular states in combination, represented as follow: S_1S_2 (sensitive to both drugs), S_1T_2 (sensitive to drug 1 and reversible resistant to drug 2), T_1S_2 (reversible resistant to drug 1 and sensitive to drug 2) and T_1T_2 (reversible resistant to both drugs). The dosage of a drug affects population dynamics in two ways: (1) reducing the net growth rate of the cells sensitive to the drug, (2) facilitating cellular state transitions from sensitivity to reversible resistance (tolerance). The irreversible and reversible drug resistance phenotypes together define nine cell types representing distinct phenotypic states.

The description of these nine stable states is shown in Table 1. The diagram of the joint model is illustrated in Fig. 1a. S_1S_2 represents the most commonly predominant cell type identified in the biopsy results when a cancer patient is first diagnosed. In our model, drug 1 (which may be a combination) corresponds to the first line treatment for this predominant cell type. Therefore, drug 1 is considered more effective against S_1S_2 cells than drug 2.

Model parameters

Supplementary Table 1 lists the 17 parameters in the joint model and their value ranges in simulations. They belong to five general categories. (1) g represents the natural net growth rate which, in these simulations is assumed to be identical for all cell types. This restriction can be relaxed by allowing different growth rates for distinct cell types. The term "natural" refers to the rate in absence of drug therapy. (2) $\alpha_1, \theta_1, \mu_1, \alpha_2, \theta_2, \mu_2$ represent the parameters pertaining to the transitions between the reversible states governed by the activities of the two pathways. Their meanings will be explained in the next section. (3) T_1 and T_2 represent the rates of acquiring irreversible resistance phenotypes to each drug by genetic change. (4) $\rho_{S_i}, i = 1, 2$ is the drug i sensitivity of sensitive cells relative to the natural net growth rate; $\rho_{T_i}, \rho_{R_i}, i = 1, 2$ denote the sensitivity for cells reversibly and irreversibly resistant to drug i, respectively; $\rho_{T_i}/\rho_{S_i}, \rho_{R_i}/\rho_{S_i}, i = 1, 2$ are the decreasing ratios of drug i sensitivity relative to the natural net growth rate for cells reversibly and irreversibly resistant to drug i, respectively. (5) R_{1ratio} and R_{2ratio} represent the fractions of cells possessing irreversible resistance of drugs 1 and 2 in the initial population. We set the cells with double irreversible resistance to be absent ($R_1R_2 = 0$) in the initial population for all simulations since all treatments are ineffective against those cells.

Cell types possessing reversible resistance alone ($\rho_{T_i}, i = 1, 2$) are less sensitive to the targeted drug compared to cell types without resistance (ρ_{S_i}, $i = 1, 2$) where $\rho_{T_i} = \rho_{S_i} \times \rho_{T_i}/\rho_{S_i}$ and $\rho_{T_i}/\rho_{S_i} < 1$. Likewise, cell types possessing irreversible resistance alone ($\rho_{R_i}, i = 1, 2$) are less sensitive to the targeted drug compared to cell types without resistance ($\rho_{S_i}, i = 1, 2$), where $\rho_{R_i} = \rho_{S_i} \times \rho_{R_i}/\rho_{S_i}$ and $\rho_{R_i}/\rho_{S_i} < 1$. To limit the total number of virtual patients, we used only 578884 virtual patients from our previous irreversible resistant only model[22], choosing ranges and values shown in Supplementary Table 1, and applying filters described therein. Parameters related to the reversible resistance mechanism were then added to each virtual patient. We selected the subset of virtual patients where $\rho_{R_i} < \rho_{T_i}, i = 1, 2$, indicating that irreversible resistance leads to a more robust and persistent effect compared to reversible resistance, while also ensuring reversible resistance emerges more quickly than irreversible resistance. This resulted in a total of 6131903 virtual patients in the joint model. Furthermore, as a convention we assume drug 1 is more effective than drug 2 in eliminating sensitive cells, hence set $\rho_{S_1} > \rho_{S_2}$. The model parameter value ranges are based on clinical, in vitro and in vivo data across a variety of cancer types and are meant to be broadly inclusive. Application to a specific cancer type and clinical scenario would involve narrower ranges as determined by measurements made in the corresponding population[22]. By including possible parameter values, we can state general conclusions across a broad range of individual virtual patients.

Modelling equations

The transition rates between sensitive and reversibly resistant cell states are defined by parameters α_i, θ_i, μ_i, i = 1, 2 as in our previous work[24]. We first briefly recapitulate the reversible part of the model. Denote y_i pathway i activity. The dynamics of $y_i(t)$ follow a first-order differential equation with production function $f(y_i, \sigma_i, \theta_i, \alpha_i)$, degradation term proportional to $y_i(t)$, relative adjustment rate δ and random noise term η_i:

$$\delta^{-1}\frac{dy_i(t)}{dt} = f(y_i, \sigma_i, \theta_i, \alpha_i) - y_i(t) + \eta_i \quad (1)$$

$f(y_i, \sigma_i, \theta_i, \alpha_i)$ depends on drug i dosage σ_i and parameters α_i, θ_i. We set $0 \le \alpha_i \le \theta_i \le 1$ to make the production function is a step-wise function[24], it is proportional to one for any y_i above threshold θ_i and to α_i for any y_i below it. $f(y_i, \sigma_i, \theta_i, \alpha_i)$ has the following form:

$$f(y_i, \sigma_i, \theta_i, \alpha_i) = A(\sigma_i, \theta_i) \times \left[\alpha_i + (1 - \alpha_i) \times H(y_i - \theta_i)\right], i = 1, 2 \quad (2)$$

where $A(\sigma_i, \theta_i)$ is a decreasing function of σ_i:

$$A(\sigma_i, \theta_i) = 1 - \sigma_i * (1 - \theta_i), i = 1, 2 \quad (3)$$

and $H(\circ)$ is the Heaviside (step) function:

$$H(x) = \begin{cases} 0, x < 0 \\ 1, x \ge 0 \end{cases} \quad (4)$$

Qualitatively, the production rate $f(y_i, \sigma_i, \theta_i, \alpha_i)$ is raised to $A(\sigma_i, \theta_i)$ if the $y_i(t)$ value exceeds a threshold θ_i, and lowered to $A(\sigma_i, \theta_i)\alpha_i$ otherwise. $A(\sigma_i, \theta_i)$ is a dampening factor which increases with threshold θ_i and decreases with drug dosage σ_i. The dynamics are described by the Brownian motion in a double-well potential $U(y_i, \sigma_i, \theta_i, \alpha_i)$:

$$U(y_i, \sigma_i, \theta_i, \alpha_i) = -f(y_i, \sigma_i, \theta_i, \alpha_i) \times (y_i - \theta_i) + \frac{y_i^2 - \theta_i^2}{2} \quad (5)$$

Equation 1 yields two steady pathway activity levels $A(\sigma_i, \theta_i)$ and $\alpha_i A(\sigma_i, \theta_i)$ corresponding to activation and inactivation of pathway i. Hence, we define the "energy gap" $\Delta E(\sigma_i, \theta_i, \alpha_i)$ between the two states as

$$\Delta E(\sigma_i, \theta_i, \alpha_i) = \kappa \times (U(A(\sigma_i, \theta_i), \sigma_i, \theta_i, \alpha_i) - U(\alpha_i A(\sigma_i, \theta_i), \sigma_i, \theta_i, \alpha_i)) \quad (6)$$

where $\kappa = 40$ for all virtual patients. Transitions between these states are stochastic events and follow a Boltzmann distribution. The transition rate from sensitive to reversible resistant cell states is:

$$\mu_{ST}^i = \mu_i \times e^{\Delta E(\sigma_i, \theta_i, \alpha_i)} \quad (7)$$

and the transition rate of the opposite direction is:

$$\mu_{TS}^i = \mu_i \times e^{-\Delta E(\sigma_i, \theta_i, \alpha_i)} \quad (8)$$

A large energy gap $\Delta E(\sigma_i, \theta_i, \alpha_i)$ increases the transition probability into the low energy state, hence elevates μ_{ST}^i and lowers μ_{TS}^i. Supplementary Figure 3 illustrates how the transition rate between sensitive and reversible resistant states changes in response to dosage adjustments. The transition rates between these reversible states thereby depend on the drug dosage. A high dosage facilitates transitions from sensitive to resistant states, while a low dosage facilitates transitions of the opposite direction. We modelled the transition between the reversible resistance and sensitive state in under the assumption of coupling between the rates as described above, which corresponds to a hypothesis of cross talk between the pathways. As an alternative formulation, these transitions could also be modeled independently using separate Hill equations. This alternative approach increases flexibility and is commonly used in pharmacological modeling, it does not have a clear mechanistic interpretation.

In the irreversible part of the model, the dynamics of a cellular population also follow a first-order differential equation. The net rate of increase of the cellular population of a phenotype is the sum of the natural net growth rate and the mutation rate into the phenotype, minus the degradation rate induced by drug dosages and the mutation rate out of the phenotype. For instance, denote $n_{i0}(t)$ and $n_{i1}(t)$ the populations of subclones without and with the irreversible resistance of drug i. Then their population dynamics follow the equations:

$$\frac{dn_{i0}(t)}{dt} = g \times [1 - \rho_{S_1} \times \sigma_1 - \rho_{S_2} \times \sigma_2 - T_i] \times n_{i0}(t) \quad (9)$$

$$\frac{dn_{i1}(t)}{dt} = g \times [1 - \rho_{x_1} \times \sigma_1 - \rho_{\bar{x}_2} \times \sigma_2] \times n_{i1}(t) + T_i \times n_{i0}(t) \quad (10)$$

x is R and $\bar{x}$ is S for $i = 1$ and x is S and $\bar{x}$ is R for $i = 2$.

The dynamic equations of the joint model are constructed by combining the reversible and irreversible parts. The equations are provided in the Supplementary Note 1. The net proliferation rate of each cellular population is the balance of production – natural growth and transitions into the designated state through irreversible and reversible resistance mechanisms – and degradation – transitions out of the designated state and reductions by drug dosages. They are illustrated in Fig.1. We also consider the degenerate models of reversible and irreversible resistance alone in Fig. 1.

Treatment strategies

The tumor size and composition in the model are governed by the dynamic equations 11-19 and drug dosage regimens $\sigma_1(t)$ and $\sigma_2(t)$. In principle, $\sigma_i(t)$ can be any temporal function with values in the normalized range [0, 1]. In practice, to better mimic the clinical setting of cancer treatment we impose several constraints on $\sigma_i(t)$: (1) $0 \le \sigma_1(t) + \sigma_2(t) \le 1 \forall t$, limiting the total normalized dosage the simulated patient receives at a given time t, as simultaneous full doses of all drugs would often be toxic to the patient. (2) $\sigma_i(t)$ takes possible values of 0, 0.5, 1, reflecting the options to administer either full or half of the

drug's recommended dosage. In clinical settings there are specific maximum doses for each drug individually and for each drug within a simultaneous combination that have been determined from clinical safety data. In these simulations, each drug is given at half-dose when used in combination with another. In general, DPM would use fixed dose combinations determined to be safe in Phase 1 studies. However, the fixed combination would differ for different drugs. (3) $\sigma_i(t)$ is a step function which changes values at the beginnings of fixed time intervals—6 weeks in our setting, also imitating the periodic administration of drugs, which often are given every 3 weeks. Moreover, radiologic evaluation would generally be no more frequent than every 6 weeks even in a clinical trial setting.

A treatment strategy is an algorithm for generating $\sigma_i(t)$'s based on the model parameter values and trajectories of population sizes before the current time point t. Ideally, we want to design a treatment sequence to (1) cure the patient (make all cellular populations vanish) if they are curable, and (2) maximize the lifespan of the patient if they are not curable. The optimal solution of $\sigma_i(t)$'s is difficult to find given the complicated governing equations and restricted temporal functions. Following our previous studies[22–24] we propose nine heuristic treatment strategies (Fig. 2). These heuristic strategies may be intuitive for oncologists.

Mono drug 1 (Mono1): treatment with continuous and constant administration of drug 1. $\sigma = (1, 0)$.

Mono drug 2 (Mono2): treatment with continuous and constant administration of drug 2. $\sigma = (0, 1)$.

Combo: treatment with continuous and constant administration of a combination of half doses of drugs 1 and 2. $\sigma = (0.5, 0.5)$.

These three static treatments, Mono1, Mono2 and Combo, are treated as benchmarks against more involved strategies.

Cycle: Periodic treatment cycling between drugs 1 and 2. The longest survival time is selected from four possible cycling treatments with combinations of two periods (3 or 6 weeks each) and opposite phases (drug 1 first or drug 2 first). The cyclic treatment is included because it achieves comparable performance to the more complex strictly optimal treatment strategy in our previous model of reversible resistance while being simpler and more practical in clinical application[24].

Strategy 0[22] *(S0)*: Current personalized medicine (CPM) strategy. Initially, it treats the virtual patient with the most effective drug on the most abundant cellular population. The nadir, a local minimum of the total cell number among the time-series profile, is set equal to the initial total population at $t = 0$, which is 5×10^9, and updated as needed at each time step. The drug is changed if either one of the following events occurs: (i) the total cell number reaches twice the nadir (equivalent to a 25% increase in linear dimensions) or (ii) the total cell number reemerges from a level below the detection threshold (10^9). If either (i) or (ii) happens and another drug has not been used, switch to another drug which means that each drug is only used once. The criteria for CPM changing drugs are similar to the established RECIST criteria for clinical progression[52]. This results in longer periods before adjustment of the treatment compared to DPM strategies.

Strategy 1[22] *(S1)*: At each time step, select the σ from $(1, 0), (0, 1)$ and $(0.5, 0.5)$ that minimizes the predicted total cell number in the next time step. This strategy is intuitive but also myopic.

Strategy 2[22] *(S2)*: Minimize the cell number of the doubly irreversible resistant cell state (R_1R_2) unless a meaningful clinical risk is imminent, and switch to minimizing the total cell number if the latter occurs. At each treatment period, select the σ from $(1, 0), (0, 1)$ and $(0.5, 0.5)$ that minimizes the predicted cell number of the incurable R_1R_2 state if the total cell number does not exceed 10^{11}. This threshold was the most effective threshold of several studied previously in terms of prolonging survival[22] under the conditions of that simulation. In actual clinical cases, many factors would determine whether the treating physician needs to prioritize immediate cytoreduction over prevention of future resistance, and in practice the physician would make this determination, using the recommendations as our model is an input in their decision making process. For example, in acute leukemia, immediate cytoreduction in an "induction period" is essential. By preventing the formation of the R_1R_2 cells, the possibility for long-term survival and/or cure is maintained. This strategy attempts to balance the long-term objective of preventing the emergence of incurable cancer cells and the short term objective of reducing (or at least controlling) the total cancer burden.

Strategy 1 cycle (S1c): Same as strategy 1 except adding two cycling treatments as options in each time step. The algorithm selects $\sigma(t)$ from three static treatments—$(1, 0), (0, 1)$ and $(0.5, 0.5)$—and two cycling treatments—3 weeks of drug 1 treatment followed by 3 weeks of drug 2 treatment in each period, and the cycling treatment with the opposite phase—to fulfill the strategy 1 objective. S1c is a composite strategy combining strategy 1 for the irreversible model and the cyclic treatment for the reversible model but using only a 3 week cycling period.

Strategy 2 cycle (S2c): Same as strategy 2 except adding the aforementioned cycling treatments as options in each time step. S2c is also a composite strategy combining strategy 2 for the irreversible model and the cyclic treatment for the reversible model but using only a 3 week cycling period.

Model simulation

We evaluate the effectiveness of the aforementioned nine strategies by conducting simulations on virtual patients with 6131903 distinct parameter configurations. The initial total cell population is 5×10^9, which roughly corresponds to a 5 cm3 lesion. The initial cell type composition is determined by parameters R_{1ratio} and R_{2ratio}. The time step of predicting responses in each strategy is set to 42 days mimicking the minimum 6 week interval between radiologic evaluations typically on clinical studies[22], which is also equivalent to two typical 3 week chemotherapy cycles.

The total simulation period is ~5 years, or 1820 days. A cellular population does not proliferate if the size is <1 cell. A tumor becomes lethal when its population size exceeds 10^{13} cells. This threshold value approximates the total cell numbers in many metastatic lesions, which often lead to mortality[22,42]. More complex functions providing a monotonically increasing risk of mortality as a function of cell number could be applied if desired. However, as the simulation is intended to encompass many different cancer types and clinical situations, it is difficult to specify such a function. Within any specific clinical application, more refined predictors of mortality could be considered. Simulation stops if the total cell number of the virtual patient exceeds 10^{13}, or if the virtual patient is cured (the cell number of each state < 1). Therefore, the survival time is either the time when the tumor size reaches the mortal threshold of 10^{13} cells or a maximum of 5 years, indicating that the tumor has either been eliminated or has not caused death within the simulation period. A treatment strategy is significantly better than another one if it shows an absolute improvement of at least 56 days (8 weeks) and a relative improvement of 25% in survival time compared to the other strategy. This is analogous to the typical minimum improvement often considered clinically significant in randomized phase 3 trials in cancer[22]. We implemented the simulation using JetStream2[66], a resource from the Advanced Cyberinfrastructure Coordination Ecosystem: Services & Support (ACCESS) program[67]. Kaplan-Meier analyses were performed using the survival analysis python library, lifelines[68].

Sensitivity analysis

Sensitivity analysis concerns how changes in input parameters affect the outcome of the simulation, which is the survival time. Denote i, j, k the indices of strategies, parameters, and virtual patients respectively, p_j the value of parameter j, and $ST_{ijk}(p_j)$ the corresponding survival time. Sensitivity value is defined as[69,70]: $S_{ijk} = |ST_{ijk}(p_j) - ST_{ijk}(p_j^-)| +$

$|ST_{ijk}(p_j) - ST_{ijk}(p_j^+)|$, where p_j^- and p_j^+ denote the decrement and increment of the parameter value p_j.

Data availability

The datasets generated and/or analyzed during the current study are available in the DPM-J repository, https://github.com/GU-DPM/DPM-J.

Code availability

Code is available at https://github.com/GU-DPM/DPM-J.

Received: 11 November 2024; Accepted: 8 June 2025;
Published online: 03 July 2025

References

1. Vasan, N., Baselga, J. & Hyman, D. M. A view on drug resistance in cancer. *Nature* **575**, 299–309 (2019).
2. Dagogo-Jack, I. & Shaw, A. T. Tumour heterogeneity and resistance to cancer therapies. *Nat. Rev. Clin. Oncol.* **15**, 81–94 (2018).
3. Michor, F., Nowak, M. & Iwasa, Y. Evolution of resistance to cancer therapy. *Curr. Pharm. Des.* **12**, 261–271 (2006).
4. Goldie, J. H. & Coldman, A. J. A mathematic model for relating the drug sensitivity of tumors to their spontaneous mutation rate. *Cancer Treat. Rep.* **63**, 1727–1733 (1979).
5. Jia, D., Jolly, M. K., Kulkarni, P. & Levine, H. Phenotypic plasticity and cell fate decisions in cancer: insights from dynamical systems theory. *Cancers* **9**, 70 (2017).
6. Bocci, F. et al. Toward understanding cancer stem cell heterogeneity in the tumor microenvironment. *Proc. Natl. Acad. Sci. USA* **116**, 148–157 (2019).
7. Bozic, I. et al. Evolutionary dynamics of cancer in response to targeted combination therapy. *Elife* **2**, e00747 (2013).
8. Beckman, R. A. & Loeb, L. A. Rare mutations in cancer drug resistance and implications for therapy. *Clin. Pharmacol. Ther.* **108**, 437–439 (2020).
9. Beckman, R. A. Neutral evolution of rare cancer mutations in the computer and the clinic. *npj Syst. Biol. Appl.* **10**, 110 (2024).
10. Marusyk, A., Janiszewska, M. & Polyak, K. Intratumor heterogeneity: the rosetta stone of therapy resistance. *Cancer Cell* **37**, 471–484 (2020).
11. Cárdenas, S. D. et al. Model-informed experimental design recommendations for distinguishing intrinsic and acquired targeted therapeutic resistance in head and neck cancer. *npj Syst. Biol. Appl.* **8**, 32 (2022).
12. Schmitt, M. W., Loeb, L. A. & Salk, J. J. The influence of subclonal resistance mutations on targeted cancer therapy. *Nat. Rev. Clin. Oncol.* **13**, 335–347 (2016).
13. Bell, C. C. & Gilan, O. Principles and mechanisms of non-genetic resistance in cancer. *Br. J. Cancer* **122**, 465–472 (2020).
14. Loeb, L. A. et al. Extensive subclonal mutational diversity in human colorectal cancer and its significance. *Proc. Natl. Acad. Sci. USA* **116**, 26863–26872 (2019).
15. Loeb, L. A., Bielas, J. H. & Beckman, R. A. Cancers exhibit a mutator phenotype: clinical implications. *Cancer Res.* **68**, 3551–3557 (2008).
16. Loeb, L. A., Springgate, C. F. & Battula, N. Errors in DNA Replication as a basis of malignant changes. *Cancer Res.* **34**, 2311–2321 (1974).
17. Beckman, R. A. & Loeb, L. A. Evolutionary dynamics and significance of multiple subclonal mutations in cancer. *DNA Repair* **56**, 7–15 (2017).
18. Gerlinger, M. et al. Intratumor heterogeneity and branched evolution revealed by multiregion sequencing. *N. Engl. J. Med.* **366**, 883–892 (2012).
19. Shaffer, S. M. et al. Rare cell variability and drug-induced reprogramming as a mode of cancer drug resistance. *Nature* **546**, 431–435 (2017).
20. Sun, C. et al. Reversible and adaptive resistance to BRAF(V600E) inhibition in melanoma. *Nature* **508**, 118–122 (2014).
21. Zhou, J., Liu, C., Tang, Y., Li, Z. & Cao, Y. Phenotypic switching as a non-genetic mechanism of resistance predicts antibody therapy regimens. *iScience* **27**, 109450 (2024).
22. Beckman, R. A., Schemmann, G. S. & Yeang, C.-H. Impact of genetic dynamics and single-cell heterogeneity on development of nonstandard personalized medicine strategies for cancer. *Proc. Natl. Acad. Sci. USA* **109**, 14586–14591 (2012).
23. Yeang, C. H. & Beckman, R. A. Long range personalized cancer treatment strategies incorporating evolutionary dynamics. *Biol. Direct* **11**, 1–25 (2016).
24. Akhmetzhanov, A. R. et al. Modelling bistable tumour population dynamics to design effective treatment strategies. *J. Theor. Biol.* **474**, 88–102 (2019).
25. Hirsh, V. Turning *EGFR* mutation-positive non-small-cell lung cancer into a chronic disease: optimal sequential therapy with EGFR tyrosine kinase inhibitors. *Ther. Adv. Med. Oncol.* **10**, 175883401775333 (2018).
26. van der Wekken, A. J. et al. Resistance mechanisms after tyrosine kinase inhibitors afatinib and crizotinib in non-small cell lung cancer, a review of the literature. *Crit. Rev. Oncol. Hematol.* **100**, 107–116 (2016).
27. Mok, T. S. et al. Osimertinib or platinum–pemetrexed in EGFR T790M–positive lung cancer. *N. Engl. J. Med.* **376**, 629–640 (2017).
28. Leonetti, A. et al. Resistance mechanisms to osimertinib in EGFR-mutated non-small cell lung cancer. *Br. J. Cancer* **121**, 725–737 (2019).
29. Brown, B. P. et al. On-target resistance to the mutant-selective EGFR inhibitor osimertinib can develop in an allele-specific manner dependent on the original EGFR-activating mutation. *Clin. Cancer Res.* **25**, 3341–3351 (2019).
30. Liu, Y. et al. Acquired EGFR L718V mutation mediates resistance to osimertinib in non-small cell lung cancer but retains sensitivity to afatinib. *Lung Cancer* **118**, 1–5 (2018).
31. Girard, N. Optimizing outcomes in EGFR mutation-positive Nsclc: which tyrosine kinase inhibitor and when?. *Future Oncol.* **14**, 1117–1132 (2018).
32. Park, K. et al. Sequencing of therapy following first-line afatinib in patients with EGFR mutation-positive non-small cell lung cancer. *Lung Cancer* **132**, 126–131 (2019).
33. Sun, J.-M. & Park, K. Can we define the optimal sequence of epidermal growth factor receptor tyrosine kinase inhibitors for the treatment of epidermal growth factor receptor-mutant nonsmall cell lung cancer?. *Curr. Opin. Oncol.* **29**, 89–96 (2017).
34. Hayashi, H. et al. Alternating therapy with osimertinib and afatinib for treatment-naive patients with EGFR-mutated advanced non-small cell lung cancer: a single-group, open-label phase 2 trial (WJOG10818L). *Lung Cancer* **168**, 38–45 (2022).
35. Goldie, J. H., Coldman, A. J. & Gudauskas, G. A. Rationale for the use of alternating non-cross-resistant chemotherapy. *Cancer Treat. Rep.* **66**, 439–449 (1982).
36. He, W., Demas, D. M., Shajahan-Haq, A. N. & Baumann, W. T. Modeling breast cancer proliferation, drug synergies, and alternating therapies. *iScience* **26**, 106714 (2023).
37. Strobl, M. A. R. et al. To modulate or to skip: De-escalating PARP inhibitor maintenance therapy in ovarian cancer using adaptive therapy. *Cell Syst.* **15**, 510–525.e6 (2024).
38. Gallagher, K. et al. Mathematical model-driven deep learning enables personalized adaptive therapy. *Cancer Res.* **84**, 1929–1941 (2024).

39. Leder, K. et al. Mathematical modeling of pdgf-driven glioblastoma reveals optimized radiation dosing schedules. *Cell* **156**, 603–616 (2014).
40. Chmielecki, J. et al. Optimization of dosing for EGFR-mutant non-small cell lung cancer with evolutionary cancer modeling. *Sci. Transl. Med.* **3**, 90ra59 (2011).
41. Gatenby, R. A., Silva, A. S., Gillies, R. J. & Frieden, B. R. Adaptive therapy. *Cancer Res.* **69**, 4894–4903 (2009).
42. Beckman, R. A., Kareva, I. & Adler, F. R. How should cancer models be constructed?. *Cancer Control* **27**, 1–12 (2020).
43. Marusyk, A. et al. Non-cell-autonomous driving of tumour growth supports sub-clonal heterogeneity. *Nature* **514**, 54–58 (2014).
44. Maltas, J. et al. Frequency-Dependent Ecological Interactions Increase the Prevalence, and Shape the Distribution, of Preexisting Drug Resistance. *PRX Life* **2**, 023010 (2024).
45. Zhang, J., Cunningham, J., Brown, J. & Gatenby, R. Evolution-based mathematical models significantly prolong response to abiraterone in metastatic castrate-resistant prostate cancer and identify strategies to further improve outcomes. *Elife* **11**, e76284 (2022).
46. Sahoo, S. et al. A mechanistic model captures the emergence and implications of non-genetic heterogeneity and reversible drug resistance in ER+ breast cancer cells. *NAR Cancer* **3**, 1–19 (2021).
47. McCoy, M. et al. Generalized evolutionary classifier for evolutionary guided precision medicine. *JCO Precis.Oncol*. **9**, e2300714 (2025).
48. Beckman, R. & Loeb, L. Genetic instability in cancer: theory and experiment. *Semin. Cancer Biol.* **15**, 423–435 (2005).
49. Pich, O. et al. The mutational footprints of cancer therapies. *Nat. Genet* **51**, 1732–1740 (2019).
50. Kuosmanen, T. et al. Drug-induced resistance evolution necessitates less aggressive treatment. *PLoS Comput. Biol.* **17**, e1009418 (2021).
51. Greene, J. M., Gevertz, J. L. & Sontag, E. D. Mathematical approach to differentiate spontaneous and induced evolution to drug resistance during cancer treatment. *JCO Clin. Cancer Inform*. **3**, 1–20 (2019).
52. Eisenhauer, E. A. et al. New response evaluation criteria in solid tumours: Revised RECIST guideline (version 1.1). *Eur. J. Cancer* **45**, 228–247 (2009).
53. Bahnassy, S. et al. 7831 Unveiling drug resistance mechanisms in triple-positive breast cancer: insights from long-term estrogen deprivation models and innovative mutation detection strategies. *J. Endocr. Soc.* **8**, bvae163.2285 (2024).
54. Bahnassy, S. et al. Unraveling vulnerabilities in endocrine therapy-resistant HER2+/ER+ breast cancer. *Endocrinology* **164**, bqad159 (2023).
55. Russo, M. et al. A modified fluctuation-test framework characterizes the population dynamics and mutation rate of colorectal cancer persister cells. *Nat. Genet* **54**, 976–984 (2022).
56. Kaufman, B. et al. Trastuzumab plus anastrozole versus anastrozole alone for the treatment of postmenopausal women with human epidermal growth factor receptor 2–positive, hormone receptor–positive metastatic breast cancer: results from the randomized phase iii tandem study. *J. Clin. Oncol.* **27**, 5529–5537 (2009).
57. Huober, J. et al. Higher efficacy of letrozole in combination with trastuzumab compared to letrozole monotherapy as first-line treatment in patients with HER2-positive, hormone-receptor-positive metastatic breast cancer – results of the eLEcTRA trial. *Breast* **21**, 27–33 (2012).
58. Rimawi, M. et al. First-line trastuzumab plus an aromatase inhibitor, with or without pertuzumab, in human epidermal growth factor receptor 2–positive and hormone receptor–positive metastatic or locally advanced breast cancer (PERTAIN): a randomized, open-label phase ii trial. *J. Clin. Oncol.* **36**, 2826–2835 (2018).
59. Ibragimova, K. I. E. et al. Outcomes for the first four lines of therapy in patients with HER2-positive advanced breast cancer: results from the SONABRE registry. *Breast Cancer Res. Treat.* **198**, 239–251 (2023).
60. Statler, A. B. et al. Real-world treatment patterns and outcomes in HR +/HER2+ metastatic breast cancer patients: a national cancer database analysis. *Sci. Rep.* **9**, 18126 (2019).
61. Razavi, P. et al. The genomic landscape of endocrine-resistant advanced breast cancers. *Cancer Cell* **34**, 427–438.e6 (2018).
62. Wang, Y.-C. et al. Different mechanisms for resistance to trastuzumab versus lapatinib in HER2- positive breast cancers - role of estrogen receptor and HER2 reactivation. *Breast Cancer Res.* **13**, R121 (2011).
63. Sudhan, D. R. et al. Extended adjuvant therapy with neratinib plus fulvestrant blocks ER/HER2crosstalk and maintains complete responses of ER+/HER2+ breast cancers: implications to the extenNET trial. *Clin. Cancer Res.* **25**, 771–783 (2019).
64. Giuliano, M. et al. Upregulation of ER signaling as an adaptive mechanism of cell survival in HER2-positive breast tumors treated with anti-HER2 therapy. *Clin. Cancer Res.* **21**, 3995–4003 (2015).
65. Gale, M. et al. Acquired resistance to HER2-targeted therapies creates vulnerability to ATP synthase inhibition. *Cancer Res.* **80**, 524–535 (2020).
66. Hancock, D. Y. et al. Jetstream2: Accelerating cloud computing via Jetstream. In *Practice and Experience in Advanced Research Computing* 1–8 (ACM, Boston MA USA, 2021).
67. Boerner, T. J., Deems, S., Furlani, T. R., Knuth, S. L. & Towns, J. ACCESS: Advancing innovation: NSF's advanced cyberinfrastructure coordination ecosystem: services & support. In *Practice and Experience in Advanced Research Computing* 173–176 (ACM, Portland OR USA, 2023).
68. Davidson-Pilon, C. lifelines: survival analysis in python. *JOSS* **4**, 1317 (2019).
69. He, W., Demas, D. M., Conde, I. P., Shajahan-Haq, A. N. & Baumann, W. T. Mathematical modelling of breast cancer cells in response to endocrine therapy and Cdk4/6 inhibition. *J. R. Soc. Interface* **17**, 20200339 (2020).
70. He, W., Shajahan-Haq, A. N. & Baumann, W. T. Mathematically Modeling the Effect of Endocrine and Cdk4/6 Inhibitor Therapies on Breast Cancer Cells. In *Computational Modeling of Signaling Networks* (ed. Nguyen, L. K.) 337–355 (Springer US, New York, NY, 2023).

Acknowledgements

This work was funded by the Department of Defense (DoD) Breast Cancer Research Program Awards W81XWH-20-1-0759 and W81XWH-20-1-0760 (to R.B.R and R.A.B., respectively). C.H.Y. was partially funded by a grant (108-2118-M-001-001-MY2) from National Science & Technology Council in the Republic of China (Taiwan). This work used Jetstream2 at Indiana University though allocation MTH240007 from the Advanced Cyberinfrastructure Coordination Ecosystem: Services & Support (ACCESS) program, which is supported by National Science Foundation grants #2138259, #2138286, #2138307, #2137603, and #2138296.

Author contributions

W.H., R.B.R., C.H.Y. and R.A.B. conceptualized and designed the study. C.H.Y. and W.H. formulated the joint model of drug resistance. W.H. developed the methodology, designed codes, performed simulation, curated data and prepared the initial draft of the manuscript. M.D.M. contributed to methodology and data curation. C.H.Y. and R.A.B. supervised and administered the project. R.B.R. and R.A.B. acquired the financial support for the study. All authors provided critical feedback and helped shape the study and the final manuscript.

Competing interests

R.A.B. is the Chief Scientific Officer of Onco-Mind, LLC, which owns patents on DPM in the European Union, Taiwan, and Japan. R.A.B. is uncompensated in this role and receives no royalties from these patents. All other authors declare no competing interests.

Additional information

Supplementary information The online version contains supplementary material available at https://doi.org/10.1038/s41540-025-00547-5.

Correspondence and requests for materials should be addressed to Wei He, Robert A. Beckman or Chen-Hsiang Yeang.